

Supporting Information

© Wiley-VCH 2010

69451 Weinheim, Germany

**Enantioselectivity of Haloalkane Dehalogenases and its Modulation by Surface Loop Engineering\*\***

*Zbynek Prokop, Yukari Sato, Jan Brezovsky, Tomas Mozga, Radka Chaloupkova, Tana Koudelakova, Petr Jerabek, Veronika Stepankova, Ryo Natsume, Jan G. E. van Leeuwen, Dick B. Janssen, Jan Florian, Yuji Nagata, Toshiya Senda, and Jiri Damborsky\**

anie\_201001753\_sm\_miscellaneous\_information.pdf

# Supporting Information

## Experimental

### Kinetic analysis

*Kinetic resolution.* Kinetic resolution experiments were performed at room temperature (21°C) as follows. Racemic substrates were added to a final concentration of 0.1 to 5 mM, depending on the apparent enzyme affinity, to screw-capped reaction vessels containing 20 ml Tris-sulphate buffer (50 mM, pH 8.2) and enzymatic reactions were initiated by adding an appropriate amount (depending on its specific activity) of purified haloalkane dehalogenase (final enzyme concentration 0.025 to 0.15 mg/ml). The progress of each reaction was monitored by periodically withdrawing samples from the reaction mixture, extracting them with diethyl ether containing 1-chlorohexane as an internal standard, drying them on a column containing anhydrous Na<sub>2</sub>SO<sub>4</sub>, and analyzing them using a Hewlett-Packard 6890 gas chromatograph equipped with a flame ionization detector and a Chiraldex B-TA or G-TA chiral capillary column (Alltech, USA). The enantiomeric ratio was calculated according to the equation  $E = (k_{cat,R}/K_{m,R})/(k_{cat,S}/K_{m,S})$ , where  $k_{cat}/K_m$  represents the specificity constant. To estimate *E*-values, the equations describing competitive Michaelis-Menten kinetics were fitted by numerical integration to time courses of changes in substrate concentrations obtained from the kinetic resolution experiments using MicroMath Scientist for Windows (ChemSW, USA). Enantioselectivity was determined by comparison of retention times and GC-MS spectra between the produced alcohol or remaining substrate enantiomer with enantiopure standards (Sigma-Aldrich, USA). Samples from kinetic resolution experiments and standards were analyzed using a Trace MS 2000 GC-MS (Finnigan, USA) equipped with a Chiraldex B-TA or G-TA chiral capillary column (Alltech, USA).

*Enzymatic Synthesis (S)-2-bromopentane.* Dehalogenation reaction was performed at a room temperature (21°C) in 24.6 l Tris sulfate buffer (50 mM, pH 8.2) containing 20% (v/v) dimethyl sulfoxide. The substrate was added to a final concentration of 2 mM. Enzymatic reaction was initiated by addition of DbjA wild-type crude extract (20 ml, 80 IU). The reaction was periodically monitored for 150 minutes and samples were analyzed by gas chromatograph equipped with a CHIRALDEX capillary GC column G-TA (Alltech, USA). When the total conversion of one enantiomer was reached, reaction was stopped by mixing with sulphuric acid decreasing pH to 4.0. The unconverted enantiomer was extracted with 20×100 ml pentane. The organic phases were anhydrous by magnesium sulphate and pentane was evaporated on rotavapor. The compounds were separated by flash column chromatography using pentane as the eluent.<sup>[1]</sup> The presence of 2-bromopentane in collected fractions was controlled by gas chromatography. Fractions containing 2-bromopentane were concentrated on rotavapor and distilled.

*Chemical Synthesis of (R)-2-bromopentane.* Optically active (*S*)-2-pentanol (0.84g, 9.53 mmol) and NaBr in 3-ml glass bottle fitted with a mechanical stirrer were cooled to -10 to -5 °C using ice-acetone bath.<sup>[2]</sup> PBr<sub>3</sub> (0.86 mg, 3.17 mmol) was added over a period of 20 min, during which time the temperature was kept between -5 and -10 °C. The reaction mixture was then stirred at -5 °C for 1 h and at 0 °C for another 1h. Then it was allowed for 15 min to warm to room temperature. The reaction mixture was neutralized by sodium bicarbonate and washed with water. Both organic and aqua's layers were extracted with pentane. Pentane layers were anhydrated by magnesium sulphate and pentane was evaporated on rotavapor. The compounds were separated by flash chromatography using pentane as the eluent. Fractions containing 2-bromopentane were concentrated on rotavapor and distilled.

*Measurement of Michaelis-Menten Constants.* Dehalogenation reactions were performed at 37 °C in 25-ml Reacti Flasks closed by Mininert Valves. The reaction mixtures were composed of 13.5 ml 50 mM Tris buffer (pH 8.2) and 1.5 ml dimethyl sulfoxide. Wide range of substrate concentrations was prepared (0.05–1.5 mM). The substrate was allowed for 30 min to dissolve. Enzymatic reaction was initiated by addition of enzyme solution (final concentration 0.15 μM). The reactions were monitored by withdrawing of 0.5 ml samples by syringe at 0, 5, 10, 15 and 20 min from the reaction mixtures. The samples were immediately mixed with 1 ml of diethyl ether. After extraction, samples were anhydrated on glass column with sodium sulphate. Samples were analyzed by gas chromatograph equipped with a CHIRALDEX G-TA or B-TA capillary GC column. Data points were measured in two independent replicates and represented as average values. Michaelis-Menten constants ( $K_m$  and  $k_{cat}$ ) were derived by non-linear curve fit employing the software Origin 6.1 (OriginLab Corp., USA).

### **Crystallographic analysis**

*Crystal structure analysis of His-tagged DbjA.* His-tagged DbjA (His-DbjA) was purified and crystallized, then diffraction data were acquired from the crystals, as previously reported.<sup>[3]</sup> The structure of His-DbjA was determined by the molecular replacement method using MOLREP,<sup>[4]</sup> and the subunit structure of DhaA (PDB code: 1BN6)<sup>[5]</sup> as a search model. The structure was refined using CNS<sup>[6]</sup> and REFMAC5<sup>[7]</sup> (**Supporting Information Table 2**). However, the crystal structure of His-DbjA showed that the His-tag was bound to the active site of the enzyme, which seemed likely to hamper preparation of the crystal of the His-DbjA-product complex. Therefore, we analyzed the crystal structure of His-tag free wild-type DbjA (DbjA).

*Crystallization and crystal structure analysis of DbjA and DbjAΔ.* In order to construct the DbjA expression vector, the *dbjA* gene was inserted into pET11a (Novagen, Germany), and the obtained vector

was named pYBJA3. The DbjA construct encodes residues 1–310 of DbjA with its C-terminus fused to a restriction site of *Sal* I with sequence Ala-Val-Asp, where Ala is residue 310 of the DbjA sequence. *E. coli*, strain BL21(DE3), was transformed with the expression vector pYBJA3 and cultured in LB medium containing 0.2% glucose and 0.2% glycerol at 37°C. The expression of DbjA was induced by adding 0.5 mM isopropyl- $\beta$ -D-thiogalactopyranoside (IPTG) when the culture reached an OD<sub>660</sub> of 0.6. After further incubation for 24 hours at 25°C the cells were harvested, washed twice with 0.1 M Glycine-NaOH buffer containing 10% (v/v) glycerol (pH 9.0), and re-suspended in the same buffer. The expressed DbjA was then purified at 4°C, as follows. The cells were disrupted by sonication (VP-30S, Taitec, Japan), after which cell debris and large particles were removed by centrifugation at 20000 x g for 30 min. The extract was diluted to 13 mg/ml and dialyzed against 0.01 M Tris-H<sub>2</sub>SO<sub>4</sub>, 10% (v/v) glycerol and 30% (w/v) ammonium phosphate (pH 7.5) for 90 min, and the resulting precipitate was removed by centrifugation at 20000 x g for 30 min. The supernatant was then dialyzed against 0.01 M Tris-H<sub>2</sub>SO<sub>4</sub>, 10% glycerol (v/v) and 50% (w/v) ammonium phosphate (pH 7.5) for 2 hours. The resulting precipitate was again collected by centrifugation at 20000 x g for 30 min, re-dissolved in 0.01 M Tris-H<sub>2</sub>SO<sub>4</sub>, 10% glycerol (v/v) (pH 7.5) (Buffer A) and dialyzed overnight against buffer A. The dialyzed enzyme solution was applied to a DEAE-Sephadex FF (Amersham Biotech, USA) column (2.6 x 15 cm) equilibrated with buffer A, which was washed with 200 ml of buffer A then eluted by a linear gradient of 0–0.4 M ammonium sulphate in buffer A (total volume 200 ml, flow rate 3 ml/min, fraction volume 3 ml). DbjA was eluted in a concentration range from 0.05 M to 0.11 M of ammonium sulphate. The DbjA-containing fractions were dialyzed against buffer A containing 50% (w/v) ammonium sulphate (pH 7.5) for 4 hours. The precipitate was collected by centrifugation at 20000 x g for 30 min, and dissolved in Buffer A then dialyzed overnight against 0.1 M glycine-NaOH containing 10% glycerol (v/v) (pH 8.6). The dialyzed enzyme was concentrated to 25 mg/ml using Amicon Ultra and Centricon ultrafiltration units (Millipore, USA) for crystallization experiments. DbjA $\Delta$  was also overexpressed in *E. coli* strain BL21(DE3). The expression vector for DbjA $\Delta$ , pYBJA2del, contains the DbjA gene coding residues 1–310, except residues 140–146, with its C-terminus fused to an Ala-His-His-His-His-His-His affinity-tag (where Ala is residue 310 of DbjA). DbjA $\Delta$  was overproduced and purified using an Ni-column (Chelating Sephadex Fast Flow, GE Healthcare, USA) as previously described.<sup>[3]</sup> The fractions containing DbjA $\Delta$  were pooled and dialyzed against 0.1 M Glycine-NaOH containing 10% glycerol (v/v) (pH 8.6). The dialyzed enzyme was concentrated to 24 mg/ml using Amicon Ultra and Centricon ultrafiltration units (Millipore, USA) for crystallization experiments. Both DbjA and DbjA $\Delta$  were crystallized at 20°C by the hanging-drop vapor diffusion method. In each case a hanging drop was prepared by mixing 1  $\mu$ l each of the protein and reservoir solution (17–19.5% (w/v) PEG 4000, 0.2 M calcium acetate, and 0.1 M Tris-HCl pH 7.9–8.1).<sup>[3]</sup> Microseeds of the His-DbjA were required for the crystallization of DbjA. Two forms of the DbjA

crystals, named DbjA(I) and DbjA(II), were obtained from the same crystallization conditions. DbjA(I) and DbjA(II) belong to the space group of  $C2$  and  $P2_1$ , respectively (**Supporting Information Table 2**). Diffraction data were collected at 100 K. Before flash cooling in an  $N_2$  stream at 100 K, crystals of DbjA and DbjA $\Delta$  were cryo-protected by soaking them in cryo-protectant solution containing 25% (*w/v*) PEG 4000, 20% (*w/v*) sucrose, 10% (*w/v*) PEG 400, 0.2 M calcium acetate and 0.1 M Tris-HCl (pH 8.0), for a few seconds. Data on DbjA and DbjA $\Delta$  structures were acquired using a Quantum 210 CCD camera at beamline NW12 of Photon Factory (PF)-AR in KEK (Tsukuba, Japan). The diffraction data were processed and scaled using the program HKL2000.<sup>[8]</sup> The crystal structures of DbjA and DbjA $\Delta$  were determined by the molecular replacement method with the program MOLREP in the CCP4 program suite,<sup>[9]</sup> using the crystal structure of His-DbjA (PDB code: 3AFI) as a search model. Crystallographic refinements were carried out using the programs CNS and REFMAC5. Water molecules with B-factors exceeding 50 Å<sup>2</sup> were removed from the coordinates. A summary of the crystallographic refinement is given in **Supporting Information Table 2**.

*Simulated annealing omit maps.* SA-omit maps were calculated using the programs CNS and REFMAC5. After the SA-refinement with CNS (1500K to 300K), further crystallographic refinement was performed with REFMAC5, and a sigmaA-weighted electron density map was calculated using the CCP4 program suite. The ( $F_{o(\text{DbjA})} - F_{o(\text{DbjA}\Delta)}$ ) difference Fourier map was prepared using the CCP4 program suite.

### **Thermodynamic analysis.**

The temperature dependence of enantioselectivity was analyzed as follows. Chiral substrates were added to a final concentration of 0.5 to 3 mM, depending on enzyme affinity, to 20 ml of glycine buffer (100 mM, pH 8.6) in 25 ml Reacti-Flasks closed by Mininert Valves, and enzymatic reactions were initiated by adding appropriate amounts of DbjA enzyme (final concentration, 0.2-2.0 μM) according to its activity with the selected substrate. The progress of the reactions was monitored by periodical withdrawing of 0.5 ml sample from the reaction mixture. The reaction was stopped by mixing the sample with 1 ml of diethyl ether containing 1,2-dichloroethane as an internal standard. After extraction, diethyl ether was dehydrated using a glass column with sodium sulphate. The samples were automatically analyzed using a Hewlett-Packard 6890 gas chromatograph (Agilent, USA) equipped with a flame ionization detector and a Chiraldex B-TA or G-TA chiral capillary column (Alltech, USA).

The difference in activation enthalpy and entropy between enantiomers, denoted  $\Delta_{R-S}\Delta H^\ddagger$  and  $\Delta_{R-S}\Delta S^\ddagger$ , respectively, was determined by studying the variation of the enzyme enantiomeric ratio with temperature, Equation 1.

$$\ln E = -\frac{\Delta_{R-S}\Delta H^\ddagger}{R} \cdot \frac{1}{T} + \frac{\Delta_{R-S}\Delta S^\ddagger}{R} \quad (1)$$

where  $R$  is the universal gas constant and  $T$  is absolute temperature. Since free ( $R$ )- and ( $S$ )-enantiomers of the same substrate have identical enthalpies and entropies, the activation enthalpy and entropy differences can be replaced by relative enthalpies ( $H^\ddagger$ ) and entropies ( $S^\ddagger$ ) of the rate-limiting transition states of the enzyme-catalyzed reaction as

$$\Delta_{R-S}\Delta H^\ddagger = \Delta_{R-S}H^\ddagger = H_R^\ddagger - H_S^\ddagger \quad (2a)$$

$$\Delta_{R-S}\Delta S^\ddagger = \Delta_{R-S}S^\ddagger = S_R^\ddagger - S_S^\ddagger \quad (2b)$$

Since  $\ln E$  varies linearly with the reciprocal temperature the magnitudes of  $\Delta_{R-S}\Delta H^\ddagger / R$  and  $\Delta_{R-S}\Delta S^\ddagger / R$  were determined as the slope and intercept of this line, respectively. The racemic temperature ( $T_r$ ) was determined as the ratio of the differential activation enthalpy and entropy, Equation 3.

$$T_r = \frac{\Delta_{R-S}\Delta H^\ddagger}{\Delta_{R-S}\Delta S^\ddagger} \quad (3)$$

## Computational analysis

**Molecular docking.** Substrates were docked in the active sites of wild-type DbjA, DbjA $\Delta$  and DbjA $\Delta$ +His139Ala using the program AUTODOCK 3.05.<sup>[10]</sup> The structures of DbjA (PDB code 3A2M) and DbjA $\Delta$  (PDB code 3A2L) originated from crystallographic analysis. The substitution His139Ala was introduced to DbjA $\Delta$ +His139Ala by the program Pymol 0.99 (DeLano Scientific, San Francisco). Hydrogen atoms were added to these proteins by the program WHATIF 6.0.<sup>[11]</sup> The grid maps were calculated using AUTOGRID 3.06 for all atom types occurring in the substrates,<sup>[10]</sup> with range set to 81 x 81 x 81 grid points and 0.25 Å spacing, centred at the nucleophilic oxygen atom of Asp103 to cover the whole active site of the enzymes. 250 docking calculations were performed for both substrates. The Lamarckian Genetic Algorithm was used with a population size of 250 individuals, a maximum of 1.5 x 10<sup>6</sup> energy evaluations and 27,000 generations, elitism value 1, mutation rate 0.02 and cross-over rate 0.8. The local search was based on the pseudo Solis and Wets algorithm with a maximum of 300 iterations per local search.<sup>[12]</sup> Final orientations from every docking were clustered with a clustering tolerance for the root-mean-square positional deviation of 0.5 Å.

*Molecular dynamics (MD) simulations.* Starting structures for MD simulations were generated from the docked structures (binding modes) of each enzyme complexed with investigated substrates. The addition of three Na<sup>+</sup> ions to this selection resulted in a zero total charge of a 23 Å-radius simulation sphere centered at the O<sub>D1</sub> atom of Asp103. All residues further than 18 Å from the center of the simulation sphere were electroneutral. The water molecules were added to the simulated system by immersing the simulation sphere into the sphere of TIP3P water molecules subjected to the surface-constraint all-atom solvent type boundary condition.<sup>[13]</sup> These boundary conditions were designed to mimic the average polarization and density of surface water molecules as if these molecules were part of the bulk aqueous solution. Positions of water molecules in the active site were taken from the crystal structure. Positions of atoms lying outside the sphere boundary were fixed at their crystallographic positions, and their non-bonded interactions with the atoms within the simulation sphere were turned off. The structures of the simulated systems were equilibrated by a gradual heating of the simulated system from 5K to 298K in a series of twelve MD simulations with gradually increasing step sizes (0.5 to 2 fs) and 190 ps simulation time in total. The energies were sampled every 10 steps. The SHAKE algorithm was applied to hydrogen atoms of both solute and solvent molecules.<sup>[14]</sup> The non-bonded interactions were evaluated explicitly for distances shorter than 10 Å. The local reaction field method was used to include long-range electrostatic interactions for distances beyond a 10 Å cut-off.<sup>[15]</sup> The long-range potential was updated every 40 steps. All MD simulations were carried out using the program Q.<sup>[13b]</sup>

*Binding free energy calculations.* Five different snapshots were selected from the equilibrated trajectory for each binding mode as starting structures for five independent binding free energy calculations. The reference system consisted of substrate molecule in the 23 Å radius sphere of TIP3P water molecules. MD simulations of 3 ns length for all five starting structures and reference aqueous system were carried out at 298K using 2 fs step-sizes. Binding free energies ( $\Delta G_{bind}^{LRA}$ ) were calculated using the linear response approximation (LRA/ $\alpha$ ) method.<sup>[16]</sup> In this approximation,  $\Delta G_{bind}^{LRA}$  is evaluated from average energies  $\langle U \rangle$  of the substrate ( $l$ ) sampled from MD trajectories calculated in the protein ( $p$ ) and water ( $w$ ) as

$$\Delta G_{bind}^{LRA/\alpha} = \beta(\langle U_{elec,l}^p \rangle_l - \langle U_{elec,l}^w \rangle_l) + \alpha(\langle U_{vdw,l}^p \rangle_l - \langle U_{vdw,l}^w \rangle_l) + \beta \langle U_{elec,l}^p \rangle_l \quad (4)$$

where subscripts  $elec,l$  and  $vdw,l$  denote electrostatic and van der Waals components of the interaction energy of  $l$  with its protein and/or water environment,  $\alpha$  and  $\beta$  are empirical constants, and  $\langle \rangle_l$  is the MD trajectory obtained with all atomic charges on  $l$  set to zero. The parameter  $\alpha$  was adjusted to 0.56 by comparing the observed and calculated hydration free energies for imidazole, difluorotoluene, and protonated cytosine as representative of non-polar, polar and charged solutes, respectively.<sup>[16b]</sup> The

parameter  $\beta = 0.5$  is a theoretical parameter that relies on the validity of the electrostatic linear-response theory.<sup>[17]</sup> The binding free energies for individual binding modes were obtained as averages over all stable trajectories selected from five independent calculations, as described above.

*Near Attack Configuration (NAC) analysis.* The presence of NACs along calculated MD trajectories was evaluated every 0.5 ps using a two-parameter geometric condition proposed by Hur and Bruice for this reaction class.<sup>[18]</sup> More specifically, two parameters characterizing NAC states were defined: (i) the distance between the nucleophilic oxygen and the attacked carbon atom  $\leq 3.5$  Å and (ii) the angle formed by the nucleophilic oxygen, attacked carbon and leaving bromine had to exceed 140 degrees.

## Results

### Kinetic analysis

*Kinetic resolution.* Three different haloalkane dehalogenases were tested for their ability to resolve kinetically a series of racemic substrates (**Supporting Information Table 1**). The magnitude of the chiral resolution (*E*-values) was low for most of the substrates, but all tested dehalogenases showed excellent enantioselectivity with  $\alpha$ -bromoesters. This experiment demonstrates, for the first time, that certain enzymes of this family possess high enantioselectivity. The enzyme DbjA also showed strong enantioselectivity with  $\beta$ -substituted bromoalkanes, with preferences for converting the (*R*)-enantiomers of 2-bromopentane, 2-bromohexane, 2-bromoheptane, methyl 2-bromopropionate, ethyl 2-bromopropionate, methyl 2-bromobutyrate and ethyl 2-bromobutyrate.

**Supporting Information Table 1** Kinetic resolution of a series of racemic substrates by DhaA, LinB and DbjA.

Substrate	Enzyme					
	DhaA		LinB		DbjA	
	<i>E</i> -value	Act. <sup>a</sup>	<i>E</i> -value	Act. <sup>a</sup>	<i>E</i> -value	Act. <sup>a</sup>
2-chlorobutane	n.d.	n.d.	1	0.1	n.d.	n.d.
2-bromobutane	2	0.2	2	0.7	1	0.8
2-bromopentane	7	0.5	16	0.4	145	0.1
2-bromohexane	4	0.3	12	0.3	68	0.5
2-bromoheptane	3	0.6	3	1.4	28	1.2
1,2-dichloropropane	n.d.	n.d.	n.d.	n.d.	n.d.	n.d.
1,2-dibromopropane	1 <sup>b</sup>	n.r.	1	3.9	3	2.3
1-bromo-3-chloro-2-methylpropane	2 <sup>b</sup>	n.r.	2	3.9	1	2.3
1,2-dichlorobutane	n.d.	n.d.	n.d.	n.d.	n.d.	n.d.
1,3-dichlorobutane	2	0.2	3	0.9	1	0.4
1,2-dibromobutane	2 <sup>b</sup>	n.r.	10	2.1	3	1.9
1,3-dibromobutane	1	0.2	5	1.4	1	1.4
epibromohydrin	1	0.8	1	0.6	2	0.3

methyl 2-bromopropionate	>200	1.5	52	7.7	>200	2.6
ethyl 2-bromopropionate	85	2.3	97	6.5	>200	15.9
methyl 2-bromobutyrate	n.d.	n.d.	28	1.3	>200	0.01
ethyl 2-bromobutyrate	>200	0.1	>200	13.3	>200	0.3
methyl 3-bromo-2-methyl propionate	5 <sup>b</sup>	n.r.	3	6.6	20	2.1
ethyl 3-bromo-2-methyl propionate	4	1.8	1	5.2	20	4.6
methyl 2,4-dibromobutyrate	1	0.1	2	0.8	1	0.7
<i>trans</i> 1,2-dibromocyclohexane	n.d.	n.d.	3	0.03	n.d.	n.d.
2-bromo-1-phenylpropane	1	0.3	2	0.5	2	0.2

<sup>a</sup> specific activity in  $\mu\text{mol}\cdot\text{min}^{-1}\cdot\text{mg}^{-1}$  of enzyme; <sup>b</sup> data from Pieters *et al.*; <sup>[19]</sup> n.d. ... no activity detectable (below the detection limit of  $0.5\text{ nmol}\cdot\text{min}^{-1}\cdot\text{mg}^{-1}$  of enzyme); n.r. ... not reported

*Synthesis of (S)- and (R)-2-bromopentane.* (*S*)- and (*R*)-enantiomer of 2-bromopentane were synthesized enzymatically by DbjA and chemically, respectively. The purity of the products was controlled by 400 MHz NMR and gas chromatography. Enantiomeric excess was determined by gas chromatograph equipped with a CHIRALDEX capillary GC column B-TA. The kinetic resolution of 2-bromopentane yielded 0.86 g (21%) of (*S*)-enantiomer with an enantiomeric excess of >99%. The chemical purity was 86%. The poor solubility of 2-bromopentane was improved by addition of organic co-solvent dimethyl sulfoxide 20% (v/v). The organic synthesis of 2-bromopentane yielded 0.34 g (24%) of (*R*)-enantiomer with an enantiomeric excess of 93%. The chemical purity was 92%.

### Crystallographic analysis

*Two crystal forms of DbjA.* Crystal structures of DbjA were determined in two distinct space groups, *C*2 and *P*2<sub>1</sub> (**Supporting Information Table 2**), designated types I [DbjA(I)] and II [(DbjA(II))], respectively. Crystals of types I and II respectively contain one and two dimers in the asymmetric unit. Notably, one subunit of DbjA(II), subunit E, showed significantly higher temperature factors than other subunits (A, B and F) and thus poor electron density. Since resolution of the crystal and *R*-factor/free *R*-factor of DbjA(I) are significantly better than those of DbjA(II), the crystal structure of DbjA(I) was mainly utilized for the structural comparison with DbjA $\Delta$ .

*Structure of DbjA.* The main domain of DbjA comprises residues 6-144 and 240-308 and shows the typical features of  $\alpha/\beta$ -hydrolases. The cap domain is composed of five  $\alpha$ -helices, formed from residues 145-216. The overall structure of DbjA is very similar to that of other haloalkane dehalogenases, such as LinB and DhaA, except for its additional residues, 140-150, which form a loop between the main and cap domains and part of the first  $\alpha$ -helix of the cap domain (residues 145-150). Thus, the loop between the main and cap domains and the first  $\alpha$ -helix of the cap domain are longer than corresponding regions of

DhaA and LinB. The DbjA $\Delta$  has deleted residues 140-146. The residues 147-150 form a loop in DbjA $\Delta$  (**Figure 1a,b**).

*Alternative conformations of His139.* The crystallographic refinement suggested that the side-chains of His139 in both subunits A and B of DbjA(I) adopt alternative conformations (**Figure 1c,d**), and this was confirmed using  $F_o-F_c$  SA-omit maps. The SA-omit map that was calculated using the DbjA structure with the inclined conformation gave a significant density ( $> 3.0 \sigma$  level) around the side-chain of the deflected conformation, and *vice versa*. We thus concluded that His139 in each subunit of DbjA(I) adopts both alternative conformations.

In the DbjA(II) crystal the situation is slightly different. The His139 of subunit B showed both conformations, but the His139 residues of other subunits consistently adopted the inclined conformation. The difference in the crystal packing between  $C2$  and  $P2_1$  might affect the difference of the His139 conformation between types I ( $C2$ ) and II ( $P2_1$ ) crystals.

**Supporting Information Table 2** Crystallographic data summary.

	His-DbjA	DbjA(I)	DbjA(II)	DbjA $\Delta$
<b>Bound product</b>	product free	product free	product free	product free
<b>Data collection</b>				
Light source	PF BL5A	PF-AR NW12	PF-AR NW12	PF-AR NW12
Space group	$P2_12_12$	$C2$	$P2_1$	$C2$
Cell dimensions				
$a, b, c$ (Å)	212.86, 117.84, 55.80	125.27, 48.69, 106.50	125.53, 47.67, 99.41	125.55, 48.65, 106.82
$\alpha, \beta, \gamma$ (°)	90, 90, 90	90, 97.36, 90	90, 93.61, 90	90, 97.93, 90
Resolution (Å)	35.18-1.75 (1.81-1.75)	33.71-1.84 (1.92-1.85)	32.82-1.89 (1.96-1.89)	43.19-1.78 (1.84-1.78)
$R_{\text{merge}}$	0.041 (0.175)	0.063 (0.254)	0.062 (0.187)	0.072 (0.349)
$I / \sigma$	14.0	10.7	14.9	10.8
Completeness (%)	95.2 (90.7)	99.9 (99.3)	99.5 (99.9)	98.6 (92.4)
Redundancy	6.1 (5.6)	4.8 (3.4)	4.8 (4.8)	3.5 (2.7)
<b>Refinement</b>				
Resolution (Å)	35.18-1.75	33.71-1.84	33.71-1.89	43.18-1.78
No. reflections	127,902	52,726	94,703	57,853
$R_{\text{work}}$	0.168	0.154	0.201	0.169
$R_{\text{free}}$	0.193	0.187	0.243	0.205
<b>No. atoms</b>				
Protein	9,299	4,681	9,308	4,544
Ligand/ion	124/4	46/2	0/3	52/2

Water	1,121	450	499	379
<b>B-factors</b>				
Protein ( $\text{\AA}^2$ )	18.9	18.8	29.8	19.4
Ligand/ion ( $\text{\AA}^2$ )	22.3/15.5	23.5/16.2	0/12.6	28.6/17.6
Water ( $\text{\AA}^2$ )	29.6	30.4	30.6	29.6
<b>R.m.s deviations</b>				
Bond lengths ( $\text{\AA}$ )	0.012	0.014	0.015	0.013
Bond angles (deg)	1.291	1.490	1.442	1.403
<b>PDB code</b>	3AFI	3A2M	3A2N	3A2L

The highest resolution shell is shown in parenthesis.

The  $F_o-F_c$  map of DbjA $\Delta$  showed a large region of electron density adjacent to the side chain of His139 in subunit A. However, adoption of the deflected conformation of His139 in subunit A could not be confirmed using the SA-omit map. The SA-refinement starting from the deflected conformation resulted in the inclined conformation. This type of conformational instability during the SA-refinement was not observed in DbjA(I). We could not therefore add the alternative conformations of His139 in subunit A of DbjA $\Delta$ . However, the additional electron density adjacent to His139 of subunit A suggests that the deflected conformation may occur in DbjA $\Delta$ , albeit at significantly lower occupancy than in DbjA(I). It should be noted that the  $F_o-F_c$  region of enhanced electron density adjacent to His139 in subunit A was also observed in the electron densities calculated from the diffraction data of another crystal (data not shown).

In order to further confirm the conformational differences of His139 between DbjA(I) and DbjA $\Delta$ , a difference Fourier analysis was performed. The  $F_{o(\text{DbjA(I)})} - F_{o(\text{DbjA}\Delta)}$  difference Fourier map showed differences in electron densities, suggesting the conformational difference of His139 between DbjA(I) and DbjA $\Delta$  (**Figure 1c**). The deflected conformation of His139 in DbjA $\Delta$  seems to have much lower occupancy than that of the His139 of DbjA(I). This result seems to be consistent with the results of the  $F_o-F_c$  SA-omit map described above. Taken together, it is highly likely that the deletion of the loop region between the main and cap domains (residues 140-146) changes the conformation of His139; the alternative conformations observed in DbjA(I) could not be clearly observed in DbjA $\Delta$ , and the inclined conformation of His139 is the major conformation in DbjA $\Delta$ .

Structural comparison of DbjA and DbjA $\Delta$  suggested that structural differences in the loop region connecting the cap and main domains are responsible for the conformational difference of His139 described above. There is enough space to accommodate the deflected conformation of His139 in DbjA (**Figure 1d**). However, the deletion of the loop region (residues 140–146) changes the structure around the active site, resulting in reduction of the volume of the space to accommodate the deflected His139.

The N atom of Gln147 and the C $\beta$  atom of Ala150 seem to make close contacts with deflected His139, avoiding the deflected conformation of His139 in DbjA $\Delta$  (**Figure 1d**).

### Thermodynamic analysis

The enantioselectivity of DbjA, DbjA $\Delta$  and DbjA $\Delta$ +His139Ala for selected representatives of  $\alpha$ -bromoesters and  $\beta$ -bromoalkanes was thermodynamically analyzed to obtain indications of enzyme- and substrate-dependent differences among the transition states of the dehalogenation reactions.

For methyl 2-bromobutyrate, all three enzyme variants showed similar reductions in their enantioselectivity with increasing temperature (**Figure 2a**). The stabilization of the rate-limiting transition state of (*R*)-enantiomers of methyl 2-bromobutyrate, which is reflected in the observed enantioselectivities (**Figure 2b**), is due to their lower transition state enthalpies, compared to those of the (*S*)-enantiomers (**Figure 2b**). This enthalpic stabilization is partly compensated by the larger entropy of the transition state for (*S*)-enantiomers. Such enthalpy-entropy compensation is consistent with reactions of (*R*)- and (*S*)-enantiomers proceeding via similar transition state structures, which are tightly bound by the enzyme active site for (*R*)-enantiomers.

The enthalpic contribution to the enantioselectivity of DbjA is larger for 2-bromopentane than for methyl 2-bromobutyrate (**Figure 2b**), but it is countered to a larger extent by entropy, resulting in weaker enantioselectivity (**Figure 2b**). This increase in the entropic contribution is consistent with larger flexibility of 2-bromopentane within the enzyme active site. More conclusive structural interpretation of the observed variations in the entropic term is hindered by the complex nature of the differential transition state entropy, which includes contributions from restrictions in the motions of the substrate, enzyme and the solvent molecules in the transition state.<sup>[20]</sup>

Surprisingly, although deletion of the surface loop in DbjA $\Delta$  does not result in loss of the preference for the (*R*)-enantiomer, causes a reversal of the signs of  $\Delta_{R-S}\Delta H^\ddagger$  and  $\Delta_{R-S}\Delta S^\ddagger$ , manifested by an increase of its enantioselectivity with temperature for 2-bromopentane (**Figure 2a**). Such temperature dependence of enantioselectivity is quite rare.<sup>[21]</sup> The reversal of the signs of  $\Delta_{R-S}\Delta H^\ddagger$  and  $\Delta_{R-S}\Delta S^\ddagger$  indicates a change in the character of the transition state for this mutant with 2-bromopentane as substrate. For example, a chemical rate-limiting step could be significantly modified. The distinct entropic signature of the enantioselectivity of DbjA $\Delta$  is lost upon mutating the His139 residue to Ala. This finding supports the hypothesis that His139 plays a significant structural role in the enzymes' enantioselectivity, as suggested by the structural and dynamic differences between DbjA $\Delta$  and DbjA $\Delta$ +His139Ala.

The thermodynamic data obtained for all three enzyme variants show reasonable enthalpy-entropy compensation, with significant differences between methyl 2-bromobutyrate and 2-bromopentane (**Figure 2a**). The linear relationship between enthalpy and entropy is described by Equation 5:

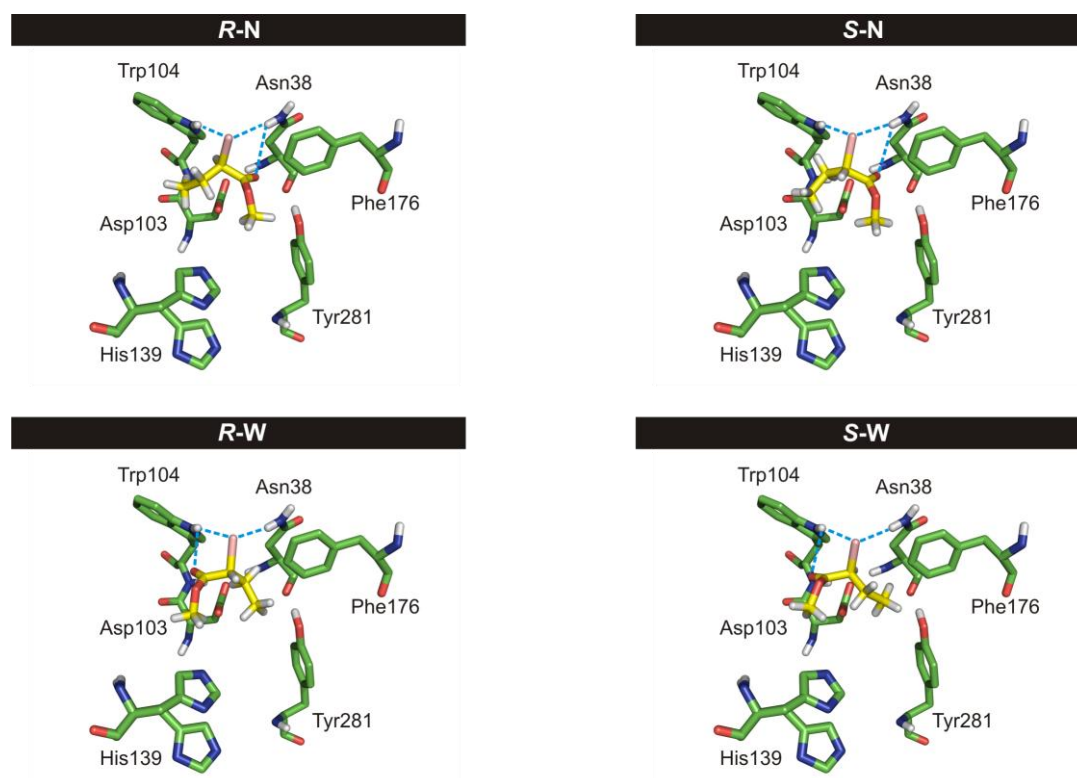
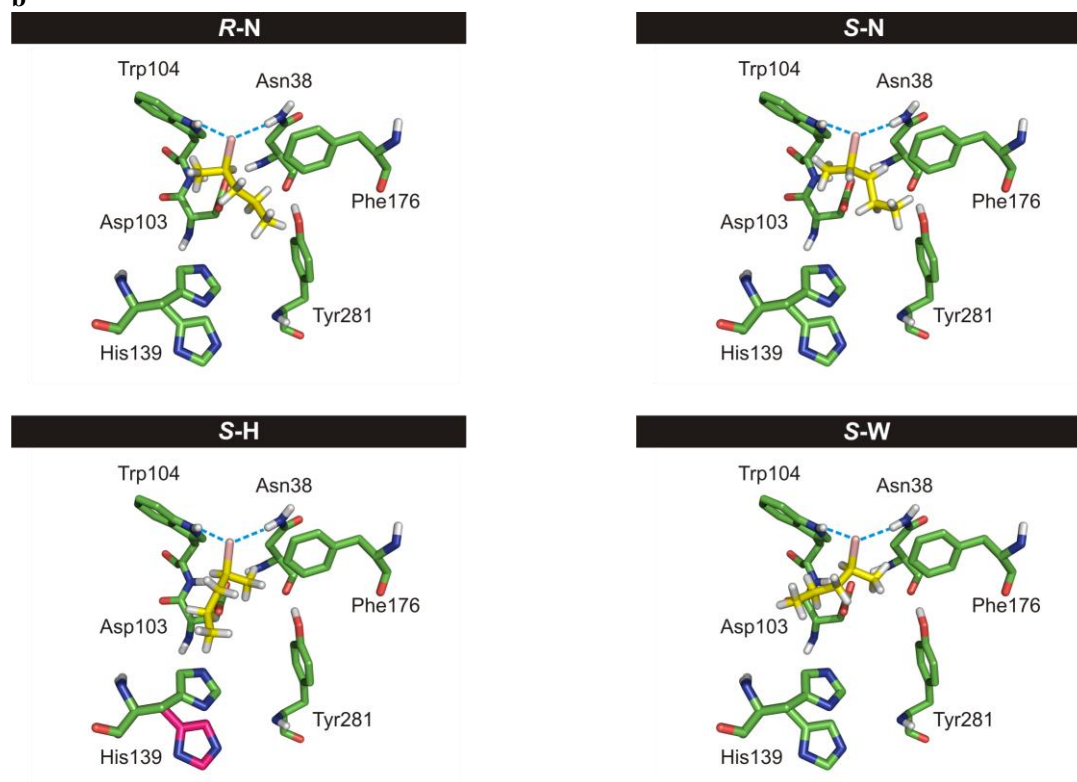
$$\Delta H = \Delta G_c + T_c \Delta S \quad (5)$$

where  $T_c$  is the compensation temperature and  $\Delta G_c$  is the Gibbs free energy at  $T_c$ . Several explanations for the compensation phenomenon have been proposed. Firstly, it may be due to the dominant role of water, as the solvent in which the processes take place. Secondly, the restricted motion of the enzyme upon binding of the substrate could be the major source of compensation; as the binding tightens the binding enthalpy will become increasingly negative, the enzyme will become more rigid and lose more entropy. Thirdly, differential solvation of the free and bound species might be responsible for the enthalpy-entropy compensation.<sup>[22]</sup> Finally, the possibility that enthalpy-entropy compensation is an artifact arising from experimental or statistical errors should also be considered. However, we observed clear differences in the temperature responses of the enzymatic enantioselectivity of DbjA, DbjA $\Delta$  and DbjA $\Delta$ +His139Ala towards 2-bromopentane and methyl 2-bromobutyrate and clear evidence of enthalpy-entropy compensation. Intense compensation was observed for kinetic resolution of 2-bromopentane, but weak for methyl 2-bromobutyrate, with all enzyme variants. This implies that the kinetic resolution of 2-bromopentane could be partly due to selective expulsion of bound solvent from the active site upon binding of enantiomeric substrates.<sup>[21b]</sup>

## Computational analysis

*Molecular Docking.* Two putatively productive binding modes were found for each enantiomer of methyl 2-bromobutyrate docked into the active sites of DbjA, DbjA $\Delta$  and DbjA $\Delta$ +His139Ala (**Supporting Information Figure 1a**). In the *R*-N and *S*-N binding modes of (*R*)- and (*S*)-enantiomers, respectively, the carbonyl group of the substrate was hydrogen-bonded to the side-chain of Asn38, which is one of the halogen-stabilizing active-site residues. Alternatively, H-bonding interaction of this carbonyl group with the side-chain of Trp104 occurred in binding modes labeled *R*-W and *S*-W.

A single putatively productive binding mode, designated *R*-N, was found for the (*R*)-enantiomer of 2-bromopentane in all investigated enzymes (**Supporting Information Figure 1b**). In contrast, as many as three possible binding modes were found for the (*S*)-enantiomer. The modes *S*-N and *S*-W are represented by complexes with the alkyl chain of the substrate in close contact with Asn38 and Trp104, respectively. The *S*-H mode, orienting the alkyl groups into close contact with His139, was obtained by docking the (*S*)-enantiomer to DbjA $\Delta$  and DbjA with the side-chain of His139 in inclined conformation. The side-chain of His139 is rotated into the active site cavity in the mutant DbjA $\Delta$ , it occupies both conformations in DbjA and is absent in DbjA $\Delta$ +His139Ala, suggesting that the interaction of the substrate with His139 favors the *S*-H binding mode. In all binding modes, 2-bromopentane displaces two structural water molecules from the active site of DbjA and DbjA $\Delta$ .

**a****b**

**Supporting Information Figure 1** Structural representations of all putatively productive binding modes of methyl 2-bromobutyrate (**a**) and 2-bromopentane (**b**) in the active sites of the studied DbjA proteins obtained from docking calculations. The ligands are in yellow sticks and the active sites in green sticks (represented by the residues Asn38, Asp103, Trp104, His139, Phe176 and Tyr281). For methyl 2-bromobutyrate, all binding modes *R-N*, *S-N*, *R-W* and *S-W* were observed, irrespective of the conformation of His139 (three H-bonds formed between substrate and halogen-stabilizing residues are indicated by dashed blue lines). For 2-bromopentane, the binding modes *R-N*, *S-N* and *S-W* were observed irrespective of the conformation of His139, while the binding mode *S-H* was not observed with His139 in the deflected conformation (in red sticks; two H-bonds formed between substrate and halogen-stabilizing residues are indicated by dashed blue lines).

*MD simulations.* All investigated binding modes of methyl 2-bromobutyrate were found stable in DbjA and DbjA $\Delta$ +His139Ala, while *R*-W and *S*-N binding modes were unstable in DbjA $\Delta$  due to increased attractive interactions with His139. The binding of the (*R*)-enantiomer is favored over the (*S*)-enantiomer by 11 kJ/mol in the wild-type DbjA, and by 10 to 7 kJ/mol in its mutants (**Supporting Information Table 3**). NAC analysis indicates that (*R*)-enantiomer is more reactive than (*S*)-enantiomer, since the (*S*)-enantiomer occurred in NAC configurations less frequently than (*R*)-enantiomer (**Supporting Information Table 3 and Supporting Information Figure 2**). The occurrence of NAC configurations has been shown to correlate with the reactivity in reactions involving nucleophilic attack on carbon,<sup>[23]</sup> and has been assumed to correlate with the reactivity in haloalkane dehalogenases.<sup>[24]</sup> Thus, in the absence of direct calculations of free energies of the transition states of the reaction catalyzed by DbjA and its mutants, we used the fraction of NAC configurations of the (*R*)- and (*S*)-enantiomers as a descriptor of their relative reactivity, based on the relationship

$$k_{\text{cat}}(R)/k_{\text{cat}}(S) = \text{NAC}(R)/\text{NAC}(S) \quad (6)$$

where NAC denotes the number of MD configurations, in which the distance between the nucleophilic oxygen and the attacked carbon atom is  $\leq 3.5 \text{ \AA}$ , and the angle formed by the nucleophilic oxygen, attacked carbon and leaving bromine is larger than 140 degrees. By combining the relative reactivity (eq. 6) and the predicted  $K_M$  values, which are related to the calculated  $\Delta G_{\text{bind}}^{\text{LRA}/\alpha}$  as  $\log K_M = -2.3RT \Delta G_{\text{bind}}^{\text{LRA}/\alpha}$ , we determined *E*-values for methyl 2-bromobutyrate for DbjA, DbjA $\Delta$  and DbjA $\Delta$ +His139Ala of 170, >13000 and 230, respectively. These predictions agree with the high enantioselectivities observed experimentally (**Figure 2b**). Experimentally observed increase in enantioselectivity of DbjA $\Delta$  towards methyl 2-bromobutyrate can be explained by more significant drop in reactivity of (*S*)-enantiomer in comparison with (*R*)-enantiomer. This drop in reactivity is due to unfavorable interactions with side-chain of His139, which is located closer to chiral center of the methyl 2-bromobutyrate in this deletion mutant.

These calculations of enantiomeric differences in binding free energies of 2-bromopentane show 5 kJ/mol preference for the (*R*)- over the (*S*)-enantiomer in the wild-type enzyme. This preference increases to 6 kJ/mol in the deletion mutant, but is negligible in the double mutant DbjA $\Delta$ +His139Ala (**Supporting Information Table 3**). The calculated preference for the (*R*)-enantiomer of 2-bromopentane further increases when NAC populations are considered because the *S*-N mode, which binds better than the *S*-H mode, shows fewer NAC configurations than the *S*-H mode and significantly fewer NAC configurations than the *R*-N mode. Thus, we can estimate enantioselectivity as follows:  $E = 71$  in DbjA,  $E = 49$  in DbjA $\Delta$ , and  $E = 79$  in DbjA $\Delta$ +His139Ala. The *E*-value calculated for wild-type DbjA would be significantly increased if the occurrence of the *S*-H binding mode with His139 in deflected conformation,

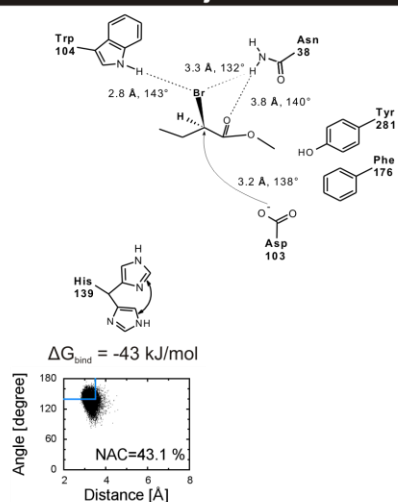
in which the stability and reactivity of (*S*)-enantiomer is diminished, was taken into account. This binding mode was not properly sampled during the MD simulations performed here due to the high time scales needed to include His139 flexibility. However, the calculated data correctly reproduce the observed decrease in enantioselectivity of the deletion mutant with 2-bromopentane. A closer analysis of the simulated trajectories of DbjA $\Delta$  shows that 2-bromopentane in *R*-N and *S*-N binding modes is repositioned in a manner that promotes interaction with the side-chain of His139, which is located closer to alkyl chain of 2-bromopentane in DbjA $\Delta$  than in DbjA. This displacement of the (*R*)-enantiomer disfavors formation of the reactive mode leading to a significant drop in enantioselectivity in this deletion mutant (NAC = 19.7% and *E* = 71 in DbjA versus NAC = 6.4% and *E* = 49 in DbjA $\Delta$ ). An additional mutation of His139 to Ala restores the *R*-N reactivity and enantioselectivity to its original level (NAC = 24.1% and *E* = 79 in DbjA $\Delta$ +His139Ala). In contrast, displacement of 2-bromopentane bound in the *S*-N mode increases its reactivity in DbjA $\Delta$  (**Supporting Information Figure 3**).

**Supporting Information Table 3** Free energies of binding ( $\Delta G_{bind}^{LRA/\alpha}$ ) and populations of near attack configurations (NACs) calculated using linear response approximations (LRA/ $\alpha$ ) for DbjA, DbjA $\Delta$  and DbjA $\Delta$ +His139Ala.

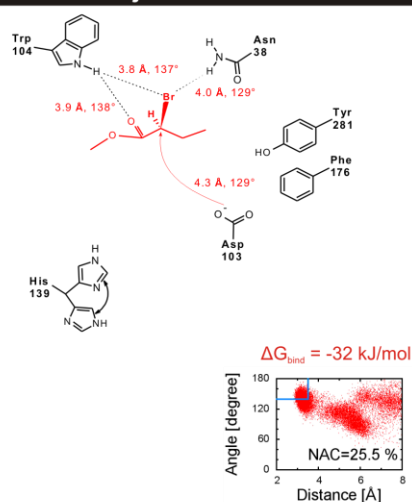
Substrate	Binding mode	Enzyme					
		DbjA		DbjA $\Delta$		DbjA $\Delta$ +His139Ala	
		NACs [%]	$\Delta G_{bind}^{LRA/\alpha}$ [kJ/mol]	NACs [%]	$\Delta G_{bind}^{LRA/\alpha}$ [kJ/mol]	NACs [%]	$\Delta G_{bind}^{LRA/\alpha}$ [kJ/mol]
methyl 2-bromobutyrate	<i>R</i> -N	43.1	-43 $\pm$ 2	5.3	-58 $\pm$ 9	40.5	-37 $\pm$ 3
	<i>R</i> -W	< 0.02 <sup>a</sup>	-31 $\pm$ 2	- <sup>b</sup>	- <sup>b</sup>	< 0.02 <sup>a</sup>	-30 $\pm$ 2
	<i>S</i> -N	< 0.02 <sup>a</sup>	-32 $\pm$ 2	< 0.02 <sup>a</sup>	-23 $\pm$ 5	< 0.02 <sup>a</sup>	-40 $\pm$ 2
	<i>S</i> -W	25.5	-32 $\pm$ 2	< 0.02 <sup>a</sup>	-48 $\pm$ 8	3.4	-29 $\pm$ 2
2-bromopentane	<i>R</i> -N	19.7	-36 $\pm$ 2	6.4	-37 $\pm$ 1	24.1	-27 $\pm$ 1
	<i>S</i> -N <sup>c</sup>	< 0.02 <sup>a</sup>	-31 $\pm$ 4	0.4	-31 $\pm$ 3	< 0.02 <sup>a</sup>	-26 $\pm$ 3
	<i>S</i> -H <sup>c</sup>	9.7	-29 $\pm$ 5	11.1	-27 $\pm$ 3	1.2	-23 $\pm$ 5

<sup>a</sup> No NACs were present among 6000 snapshots taken along a 15 ns MD trajectory. <sup>b</sup> Complex was not stable during equilibrium dynamics to allow further analysis. <sup>c</sup> *S*-N and *S*-H binding modes defined in the substrate docking calculation by AUTODOCK, may both be sampled in a single MD simulation for DbjA and DbjA $\Delta$ , but are not interchangeable in DbjA $\Delta$ +His139Ala. Thus, enantioselectivity of DbjA and DbjA $\Delta$  with 2-bromopentane was evaluated by averaging LRA/ $\alpha$  and NAC data over all *S*-N and *S*-H trajectories (30 ns), but only trajectories of the *S*-H mode (which has a higher  $k_{cat}/K_M$ ) were used to calculate the enantioselectivity of DbjA $\Delta$ +His139Ala.

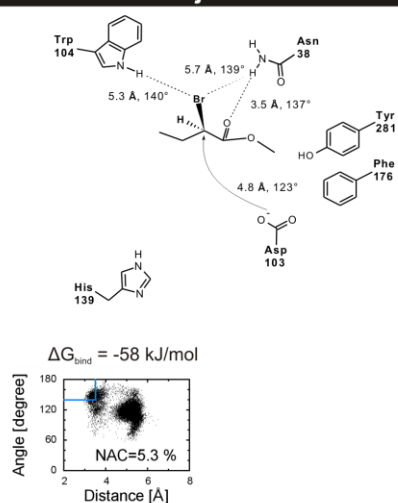
### DbjA R-N



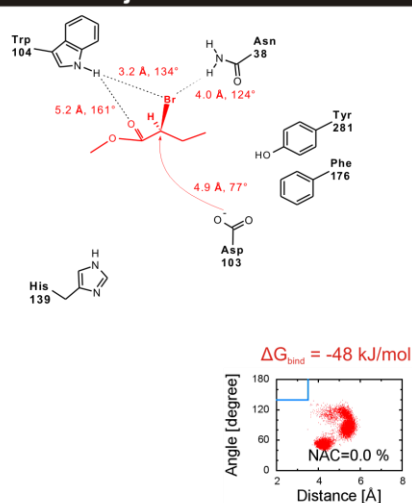
### DbjA S-W



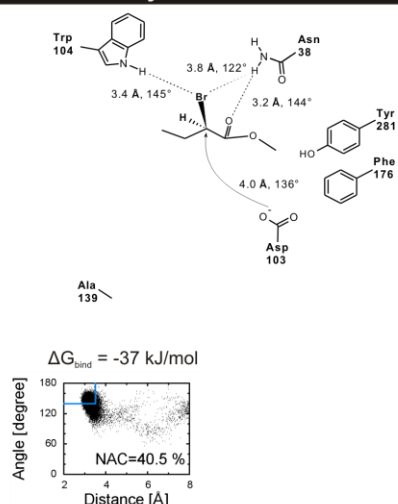
### DbjAΔ R-N



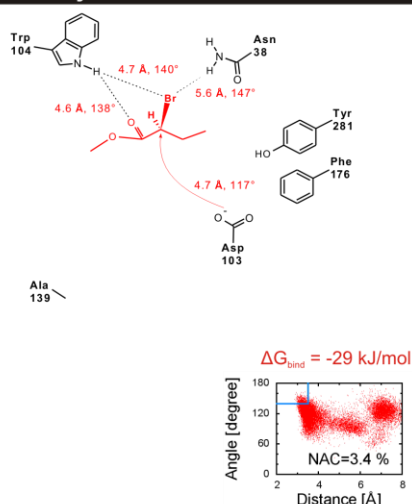
### DbjAΔ S-W



### DbjAΔ+His139Ala R-N

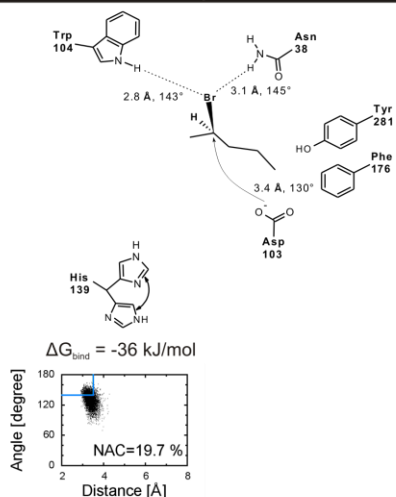


### DbjAΔ+His139Ala S-W

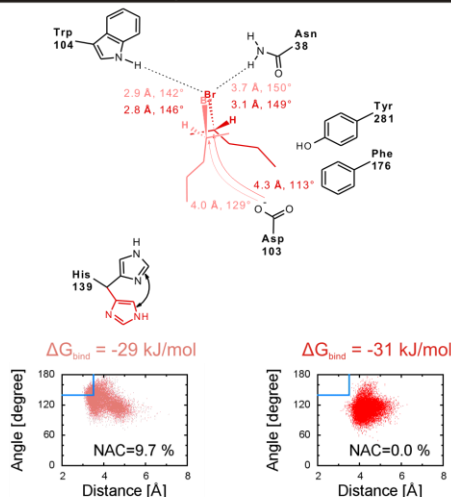


**Supporting Information Figure 2** Schematic representation of productive binding modes of methyl 2-bromobutyrate in the active sites of DbjA, DbjAΔ and DbjAΔ+His139Ala. (*R*)-enantiomer and (*S*)-enantiomer are shown in black and in red, respectively. Arrows indicate the direction of the initial nucleophilic attack. Other features displayed include: the average hydrogen-bond distances between substrate halogen and oxygen and halogen-stabilizing residues (in Å); hydrogen bond angles (in degrees), binding free energies  $\Delta G_{\text{bind}}^{\text{LRA}/\alpha}$  (in kJ/mol), NAC populations (in %) and distributions of individual structures along MD simulations (NAC parameters in blue).

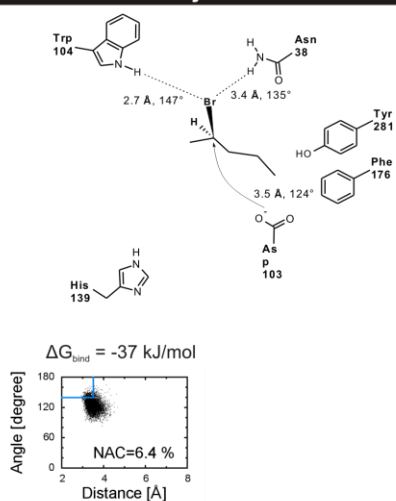
### DbjA R-N



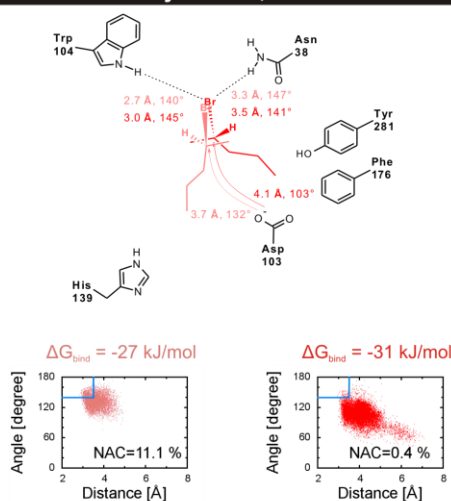
### DbjA S-H, S-N



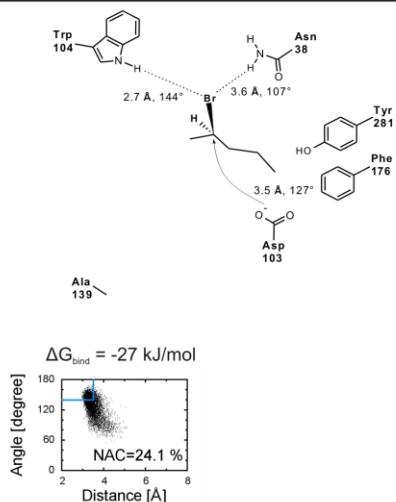
### DbjAΔ R-N



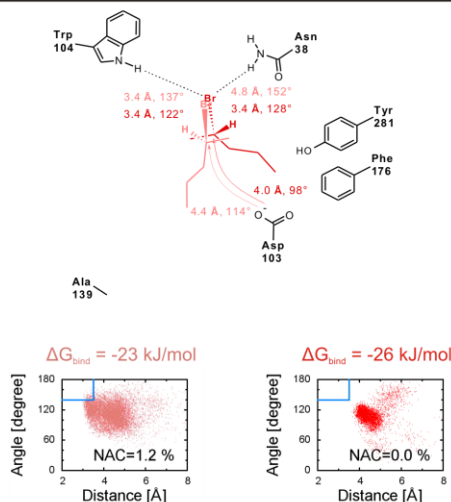
### DbjAΔ S-H, S-N



### DbjAΔ+His139Ala R-N



### DbjAΔ+His139Ala S-H, S-N



**Supporting Information Figure 3** Schematic representation of productive binding modes of 2-bromopentane in the active site of DbjA, DbjAΔ and DbjAΔ+His139Ala. (*R*)-enantiomer and (*S*)-enantiomer are shown in black and in red, respectively. Arrows indicate the direction of the initial nucleophilic attack. The average hydrogen-bond distances between substrate halogen and halogen-stabilizing residues (in Å), hydrogen-bond angles (in degrees), binding free energy  $\Delta G_{\text{bind}}^{\text{LRA}/\alpha}$  (in kJ/mol), NAC populations (in %) and distributions of individual structures along MD simulations.

## References

- [1] W.C. Still, M. Kahn, A. Mitra, *J. Org. Chem.* **1978**, *43*, 2923-2925.
- [2] R.O. Hutchins, D. Masilamani, C.A. Maryanoff, *J. Org. Chem.* **1976**, *41*, 1071-1073.
- [3] Y. Sato, R. Natsume, M. Tsuda, J. Damborsky, Y. Nagata, T. Senda, *Acta Crystallogr. Sect. F Struct. Biol. Cryst. Commun.* **2007**, *63*, 294-296.
- [4] A.A. Lebedev, A.A. Vagin, G.N. Murshudov, *Acta Crystallogr. D Biol. Crystallogr.* **2008**, *64*, 33-39.
- [5] J. Newman, T.S. Peat, R. Richard, L. Kan, P.E. Swanson, J.A. Affholter, I.H. Holmes, J.F. Schindler, C.J. Unkefer, T.C. Terwilliger, *Biochemistry* **1999**, *38*, 16105-16114.
- [6] A.T. Brünger, P.D. Adams, G.M. Clore, W.L. DeLano, P. Gros, R.W. Grosse-Kunstleve, J.S. Jiang, J. Kuszewski, M. Nilges, N.S. Pannu, R.J. Read, L.M. Rice, T. Simonson, G.L. Warren, *Acta Crystallogr. D Biol. Crystallogr.* **1998**, *54*, 905-921.
- [7] G.N. Murshudov, A.A. Vagin, E.J. Dodson, *Acta Crystallogr. D Biol. Crystallogr.* **1997**, *53*, 240-255.
- [8] Z. Otwinowski, W. Minor, in *Macromolecular Crystallography Part A* (Eds: C.W. Carter Jr., R.M. Sweet), Academic Press, **1997**, pp.307-326.
- [9] *Acta Crystallogr. D Biol. Crystallogr.* **1994**, *50*, 760-763.
- [10] G.M. Morris, D.S. Goodsell, R.S. Halliday, R. Huey, W.E. Hart, R.K. Belew, A.J. Olson, *J. Comput. Chem.* **1998**, *19*, 1639-1662.
- [11] G. Vriend, *J. Mol. Graph.* **1990**, *8*, 52-56, 29.
- [12] F.J. Solis, R.J.B. Wets, *Math. Oper. Res.* **1981**, *6*, 19-30.
- [13] a) G. King, A. Warshel, *J. Chem. Phys.* **1989**, *91*, 3647-3661; b) J. Marelius, K. Kolmodin, I. Feierberg, J. Aqvist, *J. Mol. Graph. Model.* **1998**, *16*, 213-225, 261.
- [14] J. Ryckaert, G. Ciccotti, H.J.C. Berendsen, *J. Comput. Phys.* **1977**, *23*, 327-341.
- [15] F.S. Lee, A. Warshel, *J. Chem. Phys.* **1992**, *97*, 3100-3107.
- [16] a) J. Florian, M.F. Goodman, A. Warshel, *J. Phys. Chem. B* **2002**, *106*, 5739-5753; b) J. Florián, M.F. Goodman, A. Warshel, *Biopolymers* **2003**, *68*, 286-299.
- [17] M. Born, *Z. Phys.* **1920**, *1*, 45-48; Y.Y. Sham, Z.T. Chu, H. Tao, A. Warshel, *Proteins* **2000**, *39*, 393-407.
- [18] S. Hur, K. Kahn, T.C. Bruice, *Proc. Natl. Acad. Sci. U.S.A* **2003**, *100*, 2215-2219.
- [19] R.J. Pieters, J.H. Lutje Spelberg, R.M. Kellogg, D.B. Janssen, *Tetrahedron Lett.* **2001**, *42*, 469-471.
- [20] A. Shurki, M. Strajbl, J. Villà, A. Warshel, *J. Am. Chem. Soc.* **2002**, *124*, 4097-4107.
- [21] a) V.T. Pham, R.S. Phillips, *J. Am. Chem. Soc.* **1990**, *112*, 3629-3632; b) R.S. Phillips, *J. Mol. Catal., B Enzym.* **2002**, *19-20*, 103-107; c) A.O. Magnusson, M. Takwa, A. Hamberg, K. Hult, *Angew. Chem.* **2005**, *117*, 4658-4661; *Angew. Chem. Int. Ed. Engl.* **2005**, *44*, 4582-4585.
- [22] P.L. Overbeeke, J.A. Jongejan, J.J. Heijnen, *Biotechnol. Bioeng.* **2000**, *70*, 278-290.
- [23] F.C. Lightstone, T.C. Bruice, *J. Am. Chem. Soc.* **1996**, *118*, 2595-2605.
- [24] F.C. Lightstone, Y. Zheng, T.C. Bruice, *J. Am. Chem. Soc.* **1998**, *120*, 5611-5621.